Journal of Magnetic Resonance 202 (2010) 162–172

Contents lists available at ScienceDirect

Journal of Magnetic Resonance

journal homepage: www.elsevier.com/locate/jmr

Pulse FT NMR of non-equilibrium states of half-integer spin quadrupolar nuclei in single crystals

Thomas T. Nakashima, Kristopher J. Harris, Roderick E. Wasylishen *

Department of Chemistry, Gunning/Lemieux Chemistry Centre, University of Alberta, Edmonton, Alta., Canada T6G 2G2

ARTICLE INFO

Article history:
Received 22 July 2009
Revised 3 November 2009
Available online 10 November 2009

Keywords:
Solid-state NMR
Half-integer spin quadrupolar nuclei NMR
Single crystal NMR
Pulse flip-angle effects
Non-equilibrium states

ABSTRACT

For quadrupolar nuclei with spin quantum numbers equal to 3/2, 5/2 and 7/2, the intensities of the NMR transitions in a single crystal are examined as a function of the rf excitation flip angle. Single-quantum NMR intensities are calculated using density matrix theory beginning under various non-equilibrium conditions and are compared with those determined experimentally. As a representative spin-3/2 system, the flip-angle dependence of the ^{23}Na NMR intensities of a single crystal of $NaNO_3$ was investigated beginning with the inversion of the populations associated with one of the satellite transitions. Subsequently, the populations of both satellite transitions were inverted using highly frequency-selective hyperbolic secant pulses. Calculated and experimental intensities are in good agreement. As an example of a spin-5/2 system, the flip-angle dependence of the ^{27}Al NMR transition intensities was determined using a single crystal of sapphire, Al_2O_3, starting under different nuclear spin population conditions. The experimental trends mimicked those predicted by the density matrix calculations but the agreement was not as good as for the spin-3/2 case. Some SIMPSON simulations were also carried out to confirm the results generated by our density matrix calculations. The theoretical flip-angle behavior of the NMR transition intensities obtained from a spin-7/2 spin system is also discussed.

1. Introduction

In pulse Fourier transform, FT, NMR, radio-frequency pulses are applied to a nuclear spin system to yield a free induction decay response in the time domain which is then Fourier transformed to produce the spectrum in the frequency domain [1–4]. The FT NMR experiment generally begins with the nuclear spin system at thermal equilibrium, thus the resulting NMR spectrum is representative of the true initial population differences of the energy levels involved in the transition(s). Under these conditions there is a one-to-one correspondence between the spectra generated via the FT and the continuous wave, cw, NMR methods. However, many liquid- and solid-state NMR experiments may begin in a non-equilibrium thermal state. For example, spin-tickling [5–7], difference nuclear Overhauser enhancement [8,9], chemically induced dynamic nuclear polarization CIDNP [10,11], and sensitivity enhancement experiments involving half-integer spin quadrupolar nuclei in solids [12–20], all begin with non-equilibrium conditions. In these situations, the resulting relative spectral intensities may be distorted and depend upon the observe pulse flip angle, the so-called "flip-angle effect", well known in the liquid-state NMR literature [6,21–26]. The importance of this flip-angle effect has been largely overlooked in the solid-state NMR literature except in the early application of two dimensional, 2D, nutation spectroscopy [27,28] in which the width of the rf pulse is varied as the t1 increment and the central transition is observed in the t2 domain. The shape of the resulting 2D spectrum depends upon the ratio of the quadrupolar coupling constant and the applied rf field strength.

Investigation of the "flip-angle effect" in solid-state NMR is timely, especially now that the application of sensitivity enhancement techniques for observing the central NMR transition of half-integer spin quadrupolar nuclei [12–17,19] contained in powders have become routine. These enhancement techniques require that the populations of the energy levels associated with the satellite transitions, STs, be inverted prior to observation of the central transition, CT, and therefore clearly involve a starting state that is not in thermal equilibrium.

Grandinetti et al. [29] have recently shown that the CT enhancements obtained for powdered samples using these population transfer techniques depend upon the power level used for the observe pulse. The higher the rf power of the CT conversion pulse, the lower the enhancement. The experimental observations were reproduced theoretically using numerical density matrix calculations [30].

For non-integer spin quadrupolar nuclei, single crystals serve as useful models to investigate CT enhancement experiments that involve population inversion of STs [12,13,16,17]. In these

* Corresponding author. Fax: +1 780 492 8231.
E-mail address: Roderick.Wasylishen@ualberta.ca (R.E. Wasylishen).

1090-7807/$ - see front matter © 2009 Elsevier Inc. All rights reserved.
doi:10.1016/j.jmr.2009.11.002

experiments, it is generally reported in the existing literature that a non-selective hard pulse is used but without indicating the exact flip angle [12,16,17]. When we first began using hyperbolic secant, HS, pulses [31–38] for inversion of the spin populations associated with the outer STs for sensitivity enhancement of spin-3/2 nuclei contained in single crystals, we noticed an extreme flip-angle dependence of peak intensities [12]. For example, to indicate that the populations of the satellite transitions of ^{23}Na were inverted using HS pulses, approximately a 10° non-selective observe pulse was used as shown on the left column in Fig. 1. In Fig. 1a is shown the normal ^{23}Na NMR spectrum; in 1b and 1c, the spectra obtained when the high frequency satellite and both satellite populations are inverted with HS pulses, respectively. Counter intuitively, if a non-selective 90° observe pulse is used after the high frequency satellite is inverted, the resulting spectrum would have an intensity ratio of 1.5:1.0:1.5 (Fig. 2b). Similarly, a spectrum with intensity ratio of 1.0:0.0:1.0 would result if a non-selective 90° observe pulse was applied after both satellite populations were inverted. Using selective 90° pulses as shown in the right-hand column in Fig. 1 provides the expected enhancement in CT intensity [12,13]. Nowhere in the solid-state NMR literature could we find an adequate description of the experimental pulse angle effects that we observed using non-selective pulses for single-crystal samples when the nuclear spin state did not start at thermal equilibrium.

Schmidt [39], however, and subsequently Man and coworkers [40] have reported that for a spin-3/2 system initially at thermal equilibrium, the single-quantum transitions in either a cw or non-selective pulse experiment have relative intensities 0.3:0.4:0.3 [41,42] for a quadrupolar perturbed system, with the normalized total intensity being equal to 1. For a selective 90° pulse applied to each transition, the relative intensities become 0.173:0.200:0.173, significantly smaller than those obtained in the non-selective experiment [43]. Schmidt has also calculated and tabulated the theoretical intensities for each transition for nuclei with spin quantum numbers from $I = 1/2$ to 7/2, which have been reproduced in two articles [40,43]. These calculations begin with the assumption that initially the nuclear spins are at thermal equilibrium. To our knowledge, researchers have not predicted the flip-angle dependence of the relative intensities of the transitions within systems containing spins with $I > 1/2$ when not starting from thermal equilibrium.

The success of using density matrix calculations to simulate the NMR spectra obtained from a loosely coupled two spin-1/2 spin system in liquids has been previously shown by Farrar [44,45]. In this report we wish to demonstrate that density matrix calculations can reproduce the experimentally observed flip-angle dependence of NMR peak intensities for half-integer quadrupolar nuclei of spin-3/2, -5/2, and -7/2 in single crystals starting under non-equilibrium conditions. The resulting experimental nutation curves for the spin-3/2 and -5/2 cases are first of all very interesting in themselves but also have important implications when employing sensitivity enhancement techniques for observing the NMR CT for these half-integer spin quadrupolar nuclei in powdered samples [29].

2. Theory

The magnetization behavior of a spin-1/2 system during an NMR experiment may be followed using density matrix calculations by finding the expectation values of the three spin-1/2 operators: $\boldsymbol{I}_x$, $\boldsymbol{I}_y$ and $\boldsymbol{I}_z$. For a nuclear spin system with $I > 1/2$, each

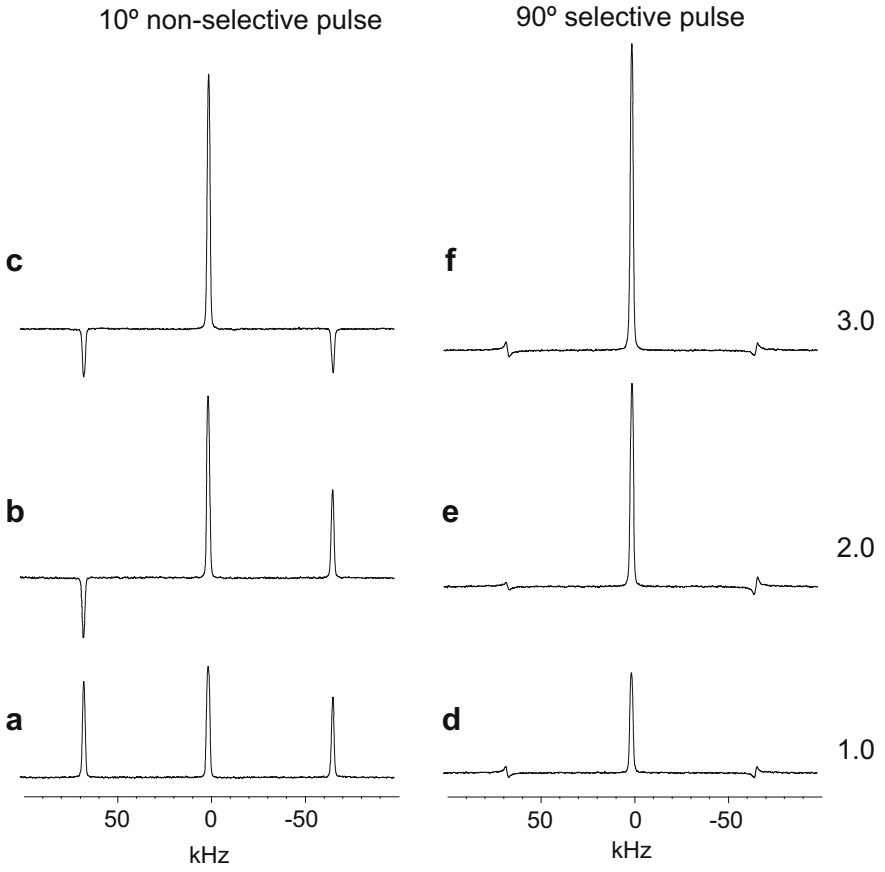

Fig. 1. ^{23}Na NMR spectra from a single crystal of $NaNO_3$ obtained with non-selective, hard pulses (left column, a–c) and with selective 90° pulses (right column, d–f); with a and d, no HS pulse applied, b and e, inversion of the populations of the high frequency satellite and c and f, with inversion of both satellite transitions. Enhancement factors are shown on the right for the selective 90° pulse experiments.

component of the magnetization may be partitioned into individual contributions which may be represented in terms of "fictitious spin-1/2 operators" [46–50]. For example, the x-magnetization, M_x, for a spin-3/2 system may be decomposed into contributions from the three single-quantum transitions associated with the two STs (i.e., $m_I = 3/2 \rightarrow m_I = 1/2$ and $m_I = -1/2 \rightarrow m_I = -3/2$) and the CT ($m_I = 1/2 \rightarrow m_I = -1/2$). The magnitude of the x-magnetization components of the STs can be found by finding their expectation values using the fictitious spin-1/2 operators $\boldsymbol{I}_x^{1,2}$ and $\boldsymbol{I}_x^{3,4}$ and for the CT with $\boldsymbol{I}_x^{2,3}$ with similar expressions for the y- and z-magnetizations. The superscripts on the operators indicate the initial, i, and final, j, energy levels using the following basis set:

$$|1> \equiv |3/2>, |2> \equiv |1/2>, |3> \equiv |-1/2> \text{ and } |4> \equiv |-3/2>. \quad (1)$$

The matrix representation for the fictitious spin-1/2 operators, $\boldsymbol{I}_x^{i,j}$, for a spin-3/2 system are given by [46,48–50]:

$$\boldsymbol{I}_x^{1,2} = \begin{pmatrix} 0 & 1/2 & 0 & 0 \\ 1/2 & 0 & 0 & 0 \\ 0 & 0 & 0 & 0 \\ 0 & 0 & 0 & 0 \end{pmatrix}; \quad \boldsymbol{I}_x^{2,3} = \begin{pmatrix} 0 & 0 & 0 & 0 \\ 0 & 0 & 1/2 & 0 \\ 0 & 1/2 & 0 & 0 \\ 0 & 0 & 0 & 0 \end{pmatrix};$$

$$\boldsymbol{I}_x^{3,4} = \begin{pmatrix} 0 & 0 & 0 & 0 \\ 0 & 0 & 0 & 0 \\ 0 & 0 & 0 & 1/2 \\ 0 & 0 & 1/2 & 0 \end{pmatrix}.$$

In the high-temperature approximation, following the notation of Man [50], the thermal equilibrium density matrix for a spin-3/2 system is given by $\rho(0) = I_z$, which may be represented as:

$$\boldsymbol{\rho}(0) = \boldsymbol{I}_z = \begin{pmatrix} 3/2 & 0 & 0 & 0 \\ 0 & 1/2 & 0 & 0 \\ 0 & 0 & -1/2 & 0 \\ 0 & 0 & 0 & -3/2 \end{pmatrix}. \quad (3)$$

The values along the diagonal reflect the excess populations within each nuclear energy level [41].

The evolution of the density matrix during pulses or delays is described by the Liouville-von Neumann equation given by [3,51]:

$$d\boldsymbol{\rho}(t)/d(t) = -i[\boldsymbol{H}, \boldsymbol{\rho}], \quad (4)$$

with the solution being:

$$\boldsymbol{\rho}(t) = e^{-i\boldsymbol{H}t}\boldsymbol{\rho}(0)e^{i\boldsymbol{H}t}, \quad (5)$$

where $\boldsymbol{H}$ represents the effective Hamiltonian during a pulse or free precession. For a non-selective pulse along the y-axis of duration t, $\boldsymbol{H}$ may be represented as $\gamma B_1 \boldsymbol{I}_y/2\pi$ when $\gamma B_1/2\pi$ (the strength of the radio frequency field) $\gg$ the internal interactions (i.e., the quadrupolar, the dipolar and/or the anisotropy of the magnetic shielding). The exponential term, i.e., $\exp(i\gamma B_1 t/2\pi)$, may be cast in matrix form and represented by the Wigner rotation matrix, $\mathscr{D}$, which for a spin-3/2 nucleus [52,53] is a 4×4 matrix given by [54]:

$$\mathscr{D} = \begin{pmatrix} C^3 & -\sqrt{3}(C^2S) & \sqrt{3}(CS^2) & -S^3 \\ \sqrt{3}(C^2S) & C^3 - 2CS^2 & S^3 - 2SC^2 & \sqrt{3}(CS^2) \\ \sqrt{3}(CS^2) & 2C^2S - S^3 & C^3 - 2CS^2 & -\sqrt{3}(C^2S) \\ S^3 & \sqrt{3}(CS^2) & \sqrt{3}(C^2S) & C^3 \end{pmatrix} \quad (6)$$

where $C = \cos(\theta/2)$ and $S = \sin(\theta/2)$. The angle θ represents the rotation angle about the y-axis of the z-magnetization following the rf pulse applied along the y-axis. The corresponding Wigner rotation matrices for $I = 5/2$, 7/2, and 9/2 (the spin-9/2 matrix was adapted from Ref. [55]) are given in the Appendix. The initial density matrix after a pulse of duration t, changes according to:

$$\boldsymbol{\rho}(t) = \mathscr{D}\boldsymbol{\rho}(0)\mathscr{D}^{-1}, \quad (7)$$

where $\mathscr{D}^{-1}$ represents the transposed complex conjugate of the rotation matrix, $\mathscr{D}$. In order to determine the intensities of each of the spin-3/2 NMR transitions, $M_x^{i,j}$, immediately after a pulse of rotation angle, θ, we simply calculate the expectation values for $M_x^{i,j}$ using the operators $\boldsymbol{I}_x^{1,2}$, $\boldsymbol{I}_x^{2,3}$, and $\boldsymbol{I}_x^{3,4}$ for the three single quantum transitions given above. The operator for the total angular momentum in the x direction, $\boldsymbol{I}_x$, in terms of the fictitious spin-1/2 operators is given by [46]:

$$\boldsymbol{I}_x = \sqrt{3}(\boldsymbol{I}_x^{1,2} + \boldsymbol{I}_x^{3,4}) + 2\boldsymbol{I}_x^{2,3}. \quad (8)$$

(An alternative description of $\boldsymbol{I}_x$, $\boldsymbol{I}_y$ and $\boldsymbol{I}_z$ is to use the raising and lowering operators as described by Man [50]). Thus, the intensities of the magnetizations expected for each transition for a spin-3/2 nucleus are proportional to [3,44–46,50,51]:

$$\langle M_x^{1,2} \rangle \propto \text{Tr}\left\{\boldsymbol{\rho}(t)\sqrt{3}\boldsymbol{I}_x^{1,2}\right\}, \quad (9)$$

$$\langle M_x^{2,3} \rangle \propto \text{Tr}\left\{\boldsymbol{\rho}(t)2\boldsymbol{I}_x^{2,3}\right\}, \quad (10)$$

and

$$\langle M_x^{3,4} \rangle \propto \text{Tr}\left\{\boldsymbol{\rho}(t)\sqrt{3}\boldsymbol{I}_x^{3,4}\right\}, \quad (11)$$

where Tr indicates the trace of the matrix resulting from the product of the density matrix after the pulse and the indicated operators.

For selective pulses, the time required for a 90° pulse, τ_{90}, must be sufficiently long such that $\tau_{90}\Delta \gg 1$, where Δ represents the frequency separation between any adjacent transitions [39]. In this case, only the selected transition will be perturbed leaving all others undisturbed. Thus, following Schmidt's treatment [39], instead of the general Wigner rotation matrix used above for a spin-3/2 system, for a non-selective excitation, to represent a selective pulse effecting a transition between $m_i \rightarrow m_j$, a 2×2 rotation matrix is used; this rotation matrix is simply the Wigner rotation matrix used for a spin-1/2 nucleus. More specifically, for a θ rotation for which the transmitter is positioned to only excite the $m_I = 3/2$ to $m_I = 1/2$ transition, the rotation matrix can be represented with the elements $\mathscr{D}_{1,1} = \mathscr{D}_{2,2} = \cos(\theta/2)$ and $\mathscr{D}_{1,2} = -\mathscr{D}_{2,1} = -\sin(\theta/2)$, as shown below:

$$\mathscr{D} = \begin{pmatrix} \cos(\theta/2) & -\sin(\theta/2) \\ \sin(\theta/2) & \cos(\theta/2) \end{pmatrix} \quad (12)$$

and for this case the initial density matrix will be:

$$\boldsymbol{\rho}(0) = \begin{pmatrix} 3/2 & 0 \\ 0 & 1/2 \end{pmatrix}. \quad (13)$$

Similarly, for selective excitation of the central transition, i.e., $m_I = 1/2 \rightarrow m_I = -1/2$, the Wigner rotation matrix is identical to Eq. 12 but the initial density matrix is:

$$\boldsymbol{\rho}(0) = \begin{pmatrix} 1/2 & 0 \\ 0 & -1/2 \end{pmatrix}. \quad (14)$$

A similar initial density matrix is created to represent the selective rotation occurring between the energy states 3–4 which corresponds to the other satellite transition. Calculations for the expectation values for the components of the x-magnetization are as described above in Eqs. (9)–(11).

The initial density matrix representing inversion of the populations of a nuclear spin state may be created by inverting the appropriate elements in the thermal equilibrium density matrix. For example, if the populations associated with ST1, or $M_z^{1,2}$, of a spin-3/2 nucleus were inverted whether by a selective HS pulse or by any other method [56], the calculations would begin with the initial density operator, in Eq. 3, with elements $\rho_{1,1}$ and $\rho_{2,2}$

interchanged, with the remaining elements unchanged as shown in the matrix below:

$$\boldsymbol{\rho}(0) = \boldsymbol{I}_z = \begin{pmatrix} 1/2 & 0 & 0 & 0 \\ 0 & 3/2 & 0 & 0 \\ 0 & 0 & -1/2 & 0 \\ 0 & 0 & 0 & -3/2 \end{pmatrix} \tag{15}$$

All calculations were performed assuming perfect, ideal inversion pulses for which no off-diagonal density matrix elements are generated, except where noted. Also, our calculations assume no relaxation of the nuclear spins during the pulses.

Under the effects of a non-selective rf pulse, general analytical equations for the nutation behavior of the *x*-magnetization associated with the satellite, $M_x^{1,2}$, and central, $M_x^{2,3}$, transitions for a spin 3/2 nucleus are proportional to the 1,2 and the 2,3 elements, respectively (see Eqs. (9)–(11)), of the density matrix after the pulse, $\boldsymbol{\rho}(t)$, and these are given by:

$$\rho_{1,2}(t) = \sqrt{3}\Big[\rho_{1,1}(0)C^5S - \rho_{2,2}(0)(C^5S - 2C^3S^3) + \rho_{3,3}(0)(CS^5 - 2C^3S^3) - \rho_{4,4}(0)CS^5\Big] \tag{16}$$

and

$$\rho_{2,3}(t) = 3\rho_{1,1}(0)C^3S^3 + \rho_{2,2}(0)(C^3 - 2CS^2)(2C^2S - S^3) + \rho_{3,3}(0)(S^3 - 2SC^2)(C^3 - 2CS^2) - 3\rho_{4,4}(0)C^3S^3 \tag{17}$$

where $\rho_{1,1}(0)$, $\rho_{2,2}(0)$, $\rho_{3,3}(0)$ and $\rho_{4,4}(0)$ represent the elements of the initial density matrix. Substituting in the various starting population distributions into Eqs. 16 and 17 and determining the values of $\rho_{1,2}(t)$ and $\rho_{2,3}(t)$ as a function of the flip angle will yield the nutation curves (see below).

3. Experimental

All experiments were performed using a Bruker Avance 300 NMR spectrometer with a standard Bruker 4 mm MAS probe. At this field strength, 7.05 T, the resonance frequencies of ^{23}Na and ^{27}Al are 79.46 and 78.27 MHz, respectively. Sodium nitrate, $NaNO_3$, was obtained commercially and single crystals were grown from a saturated aqueous solution. A sapphire rod, Al_2O_3, of about 1 cm in length and 3 mm in diameter was used for the ^{27}Al NMR study. The rod was purchased commercially. The single crystals were placed in 4 mm rotors. Four scans and a relaxation delay of 30 s were used to acquire the ^{23}Na NMR spectra and one scan was used to obtain the ^{27}Al NMR spectra. For the latter, 160 s recycle delays were necessary when optimizing the experimental parameters used for inversion of the nuclear spin populations with HS pulses. The HS pulse shapes were created with the standard software package supplied by Bruker. The density matrix calculations were performed using a PC with the standard Microsoft Excel program. The theoretical results were also duplicated using SIMPSON [57] on a cluster of nine PC processors. Experimentally determined intensities were measured as peak heights and divided by a suitable weighting factor when compared to the calculated intensities.

4. Results and discussion

4.1. Spin-3/2

A single crystal of $NaNO_3$ was placed in the magnetic field at a random orientation such that the three transitions were separated from each other by approximately 51 kHz and each having a width at half-height of approximately 1800 Hz (see Fig. 2a). Using hard rf pulses, a pw 90° array [58] was performed with the transmitter positioned directly on resonance of the CT and the higher frequency ST intensities were found to maximize simultaneously at a pulse width value of 1.75 μs. The lower frequency ST, however, maximized at a slightly longer pulse width of 2.25 μs, even though one might expect all transitions to maximize at the identical pulse width at very high power levels [39]. To eliminate off-resonance effects, the transmitter frequency was positioned on top of each resonance and the pw array was repeated. In these experiments, the selected resonance maximized in intensity at 1.75 μs, as expected. So, when starting under thermal equilibrium conditions, each resonance showed a smooth monotonic sine dependence of the peak intensity versus pulse angle with slight phase distortion at the larger pulse angles, thus showing the expected intensity versus pulse angle dependence [58].

Shown in Fig. 2 are the ^{23}Na NMR spectra obtained using a non-selective (non-sel.), 90° pulse beginning with: (a) the nuclear spin populations at thermal equilibrium, (b) inversion of the populations associated with one of the STs, using a single-frequency HS pulse prior to the observe pulse and (c) with both populations of the ST1s inverted using a double-frequency HS pulse prior to the observe pulse. The peaks for the three single-quantum transitions in the spectra shown in Fig. 2a have relative intensities of 3.15:4.00:3.15, in Fig. 2b of 3.24:2.00:3.24, and in Fig. 2c of 3.00:0.20:2.5. It is interesting to observe that with a 90° non-sel. pulse, the CT intensity is near zero when the populations associated with both of the ST1s are inverted while a −1.1:5.3:−1.0 intensity ratio is observed using a 10° pulse (Fig. 1c). This observation is consistent with those reported by Grandinetti et al. [29] for powdered samples. The intensity of the CT observed using a selective 90° pulse, however, is enhanced by a factor of three over the thermal equilibrium situation when both the populations of the outer transitions are inverted as shown on the right-hand column in Fig. 1 [12].

The pulse-angle dependence of the ^{23}Na NMR intensities from the single crystal of $NaNO_3$ starting with the populations of both ST1s inverted using a double-frequency HS pulse was determined and the results of this experiment is summarized in Fig. 3 and compared with those determined using the density matrix calculations. The experimental intensities were scaled to match the theoretical values and the scaling factor was the same for each spectrum. Agreement between theory and experiment is excellent. The rf pulse width was varied from a value of 0.2 μs in steps of 0.2 μs with a non-sel. 90° pulse equal to 2.0 μs. At very low values of the pulse angle, the outer transitions have negative intensity relative to the CT with maximum negative intensity occurring with a pulse width of 0.6 μs (a flip angle, θ, of approx. 27°) then become positive around a value of 1.0 μs (a flip angle $\theta \approx 45°$ pulse angle). The intensities continue to increase until a value of 2.0 μs corresponding to a 90° pulse. The CT intensity increases initially, maximizing in intensity at about 0.8 μs, then decreasing to near zero with a 90° pulse. The only spectra indicating that the populations of the outer transitions are inverted occur for values of the pulse flip angle between 9° and 36° (i.e., 0.2–0.8 μs) consistent with our initial observations [12].

The theoretical intensities calculated using the density matrix formalism discussed in the theory section are listed in Table 1 for each transition of a spin-3/2 nucleus as a function of the flip angle using non-selective "observe" pulses. Three initial conditions are considered. First starting from thermal equilibrium, next with the populations of one ST1, $M_z^{1,2}$, inverted and finally with both the populations of the ST1s, $M_z^{1,2}$ and $M_z^{3,4}$, inverted.

Using the density matrix calculations outlined in the theory section for selective pulses, a comparison of the relative intensity ratios obtained from a non-sel. or sel. 90^o pulse for each transition starting at thermal equilibrium is in agreement with those published by Schmidt [39]. When employing a sel. versus a non-sel. 90° pulse, we obtain a ratio of the intensities of 1.73/3.00 = 0.58

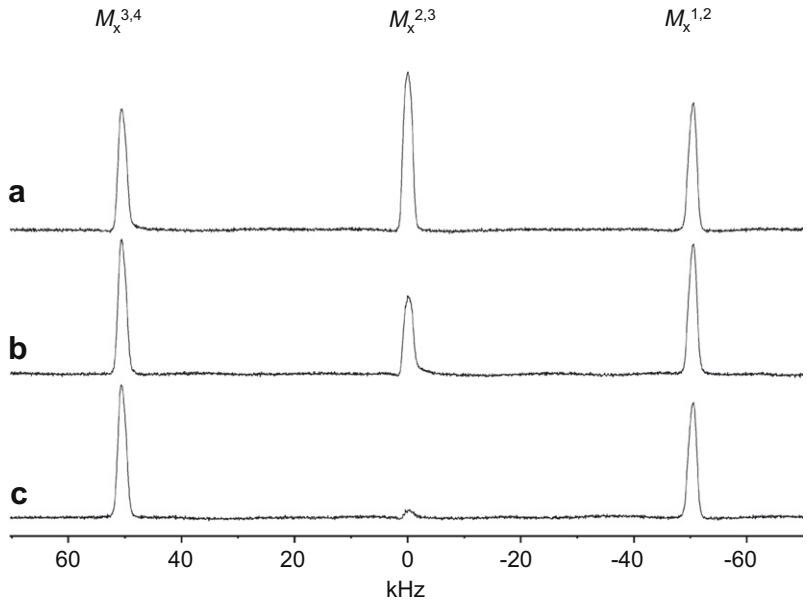

Fig. 2. ^{23}Na NMR spectra from a stationary single crystal of $NaNO_3$ determined with a 2.0 μs pulse (a non-sel. 90° pulse) starting at (a) thermal equilibrium, (b) with inversion of one ST1 using a hyperbolic secant pulse (bandwidth of 2 kHz and a duration of 1 ms) and (c) with inversion of both ST1s. Four scans per spectrum with a relaxation delay of 16 s were used. The separation between adjacent peaks is approximately 50 kHz.

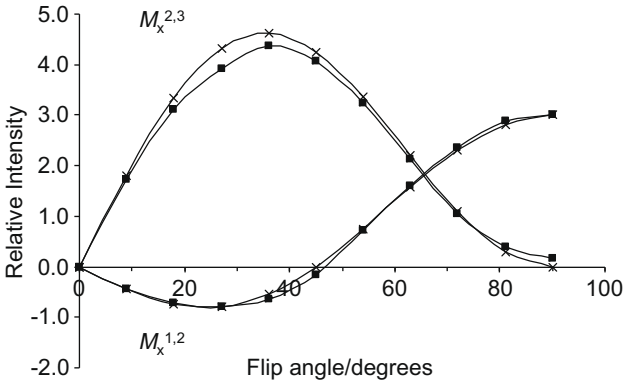

Fig. 3. Intensity plots for $M_x^{1,2}$ and $M_x^{2,3}$ for spin-3/2 nuclei starting with the populations of the transitions associated with both ST1s inverted versus pulse flip angle using non-selective pulses. Both calculated, shown as *x*'s, and observed, shown as dark squares, experimental intensity values are shown. (The experimental data is divided by 21.25 to match the calculated values.)

Table 1
Calculated intensities of the three transitions for a spin-3/2 nucleus using non-selective rf pulses from 9° to 90° under three different initial conditions.

	Thermal equil.[a]		Invert $M_z^{1,2}$			Invert[a] $M_z^{1,2}$ and $M_z^{3,4}$	
Flip angle	$M_x^{1,2}$	$M_x^{2,3}$	$M_x^{1,2}$	$M_x^{2,3}$	$M_x^{3,4}$	$M_x^{1,2}$	$M_x^{2,3}$
9°	0.47	0.63	−0.45	1.22	0.47	−0.45	1.83
18°	0.93	1.23	−0.79	2.29	0.97	−0.75	3.35
27°	1.36	1.82	−0.93	3.07	1.49	−0.80	4.32
36°	1.76	2.35	−0.82	3.48	2.03	−0.55	4.62
45°	2.12	2.83	−0.44	3.54	2.56	0.00	4.24
54°	2.42	3.23	0.16	3.30	3.01	0.75	3.36
63°	2.67	3.56	0.90	2.89	3.33	1.57	2.21
72°	2.85	3.80	1.69	2.45	3.46	2.30	1.09
81°	2.96	3.95	2.42	2.12	3.35	2.81	0.29
90°	3.00	4.00	2.99	2.00	3.00	3.00	0.00

[a] For these cases the intensity of $M_x^{1,2}$ is equivalent to $M_x^{3,4}$.

for transition $M_x^{1,2}$ and 2.00/4.00 = 0.5 for $M_x^{2,3}$; Schmidt reported identical ratios. Density matrix calculations using selective pulses were also performed beginning with the inversion of $M_z^{1,2}$ and with simultaneous inversion of $M_z^{1,2}$ and $M_z^{3,4}$. The maximum enhancement for the CT using a sel. 90° pulse occurs when the populations of both ST1s are inverted, in agreement with experiment (see Fig. 1). Using a non-sel. 90° pulse starting at thermal equilibrium yields the same intensity for the CT as using a sel. 90° with a single ST1 inversion, i.e., an intensity of 4.00. It is interesting to note, however, that in order to obtain the maximum intensity, 4.62, using a non-sel. pulse, the observe rf flip angle is 36° with both ST1s inverted; this is shown in Table 1. Finally, the intensities of $M_z^{2,3}$ shown in Fig. 1 (selective pulse) are reproduced by the density matrix calculations.

4.2. Spin-5/2

The ^{27}Al NMR spectrum obtained for a single crystal of sapphire consisted of five peaks which were separated by approximately 30 kHz, each having a width at half-height of approximately 6 kHz (see Fig. 4). Schmidt [39] and Man [40] have shown that the relative intensities of the five transitions of a spin-5/2 nucleus using either a hard pulse or obtained with a cw experiment starting from thermal equilibrium would be in a ratio of 0.143:0.228:0.257:0.228:0.143 or, more simply, 5.0:8.0:9.0:8.0:5.0. With the transmitter positioned atop the central transition, a pw 90° array was performed from 0.3 to 4.5 μs on the single crystal of sapphire and the central transition and both ST1 intensities maximized at a value of 3.6 μs with the intensities of the ST2s still continuing to increase very slowly. All of the transition intensities grew monotonically with a sinusoidal dependence with pulse width, as expected. The intensities of the five transitions using a non-selective 90° pulse were in the ratio of 6.3:8.1:9.0:8.3:6.3, close to those expected theoretically.

Shown in Fig. 4 is the ^{27}Al NMR spectra from this single crystal obtained with a non-sel. 90° pulse acquired under a series of starting conditions. Firstly, with (a) inversion of the populations of one ST1, which corresponds to inversion of $M_z^{4,5}$, second (b) with both ST1s inverted, corresponding to inversion of $M_z^{2,3}$ and $M_z^{4,5}$, and finally (c) with inversion of one side of the single crystal spectrum, i.e., with inversion of $M_z^{5,6}$ followed immediately with inversion

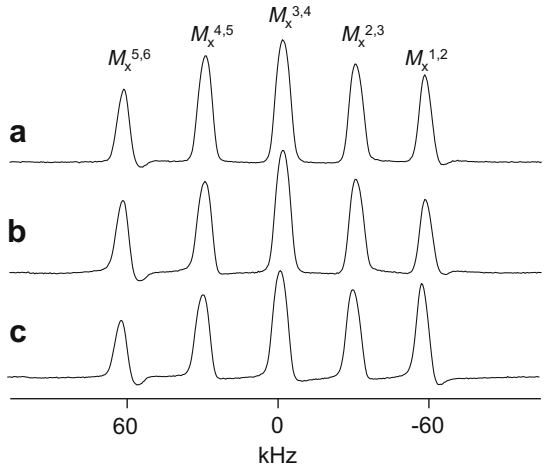

Fig. 4. The ^{27}Al NMR spectra of a single crystal of Al_2O_3 obtained with a non-selective 90° pulse with a) inversion of $M_z^{4,5}$, b) inversion of $M_z^{2,3}$ and $M_z^{4,5}$ and c) inversion of $M_z^{5,6}$ and $M_z^{4,5}$. Only a single scan was acquired for each spectrum. Inversions were performed using HS pulses of duration 5 ms with a bandwidth of about 16 kHz.

of $M_z^{4,5}$. From the spectra shown in Fig. 4 there is no indication that any of the *z*-magnetizations have been inverted prior to the "hard" observe pulse.

Listed in Table 2 are the calculated intensities of the five transitions for a spin-5/2 nucleus as a function of the flip angle using a non-selective pulse beginning with the populations at thermal equilibrium, with the populations of both ST1s inverted, and with the inversion of $M_z^{1,2}$ and $M_z^{5,6}$ followed immediately by inversion of $M_z^{2,3}$ and $M_z^{4,5}$. Also listed are the calculated intensities using the density matrix approach of each transition starting at thermal equilibrium and of the central transition, $M_x^{3,4}$, when both the populations of the ST1s are inverted, and when all the populations associated with the STs are inverted sequentially and observed using a sel. 90° pulse. The reduced intensity obtained from a sel. versus a non-sel. 90° pulse agrees with that calculated by Schmidt [39], however, he does point out that different pulse widths are necessary to effect the same pulse angle for the central transition versus the satellite transitions. The calculated relative intensities obtained from a non-sel. 90° pulse are also shown in Table 2 when only the populations of one ST1 and $M_z^{1,2}$ and $M_z^{2,3}$ are inverted. It is interesting to note that when a non-sel. 90° pulse is applied, the resulting spectra are relatively symmetric, i.e., the intensities of $M_x^{1,2} = M_x^{5,6}$ and $M_x^{2,3} = M_x^{4,5}$, regardless of the initial population distribution. The spectra shown in Fig. 4 are consistent with these calculations.

The results of the calculations also show that maximum enhancement of the CT depends not only on which outer transitions are inverted but also on the manner in which the CT is excited. For example, when observing the CT with a non-sel. pulse, maximum CT intensity, 5.62, occurs with a pulse angle of 90° with both ST1s inverted and not when both sides of the spectrum of a single crystal are inverted [19]. When observing the CT with a non-sel. pulse starting with inversion of both sides of the spectrum of a single crystal, maximum intensity of 5.22 occurs using an 18° pulse.

Shown in Fig. 5 are the experimental ^{27}Al NMR spectra of a single crystal of Al_2O_3 as a function of pulse width obtained with inversion of $M_z^{5,6}$ followed immediately by inversion of $M_z^{4,5}$ using HS pulses. The pulse widths start at 0.18 μs in steps of 0.18 μs with a pulse width of 1.8 μs corresponding to a non-sel. 90^o pulse. The intensity of the $M_x^{5,6}$ magnetization initially increases with θ, maximizing in intensity when $\theta = 27°$, then decreases to a minimum when $\theta = 54°$ and increases again with another maximum at 117°. The intensity of $M_x^{4,5}$ is negative at very small values of the pulse angle, having maximum negative intensity when $\theta = 18°$ (0.36 μs), goes through zero intensity at about 40° and increases in intensity with maximum intensity at 81°. The intensity of the CT, $M_x^{3,4}$, has two maxima of almost equal intensity occurring at approximately 30 and 90°. The intensity of $M_x^{2,3}$ increases to a maximum at around 60° and begins to decrease with increasing flip angle. The intensity of $M_x^{1,2}$ increases monotonically to a maximum at about a pulse angle of 80°.

Shown in Fig. 6 is the calculated intensity of each transition for a spin-5/2 nucleus as a function of flip angle from 0 to 180° starting with inversion of one side of the NMR spectrum of a single crystal, i.e., first the inversion of $M_z^{5,6}$ then $M_z^{4,5}$. Even though $M_z^{5,6}$ is inverted before the application of the observe pulse, it is interesting that the intensity calculated for $M_x^{5,6}$ is always positive no matter what flip angle is used for the observe pulse. This behavior was observed experimentally as illustrated in Fig. 5 as well as the small inflection point in the intensity at about a flip angle of 50° (i.e., pulse width of 1 μs). The intensity of $M_x^{4,5}$ is negative at small pulse angles with a maximum negative intensity occurring at 18°. The intensity becomes positive at about 40°, increases to a maximum at about a flip angle of 60°, and then decreases in intensity with a minimum at 90°. At 90° the intensities of $M_x^{1,2}$, $M_x^{2,3}$, $M_x^{4,5}$, and $M_x^{5,6}$ are all equal. There is a second higher maximum that occurs for the intensity of $M_x^{4,5}$ at a pulse flip angle of about 125° and the intensity decreases to zero when a 180° pulse is applied. The behavior of $M_x^{2,3}$ seems to mimic that of $M_x^{4,5}$ but in the reverse order. Likewise, the behavior of $M_x^{1,2}$ seems to mimic that of $M_x^{5,6}$ in the reverse order. A similar behavior was also reported in

Table 2
Calculated intensities of the five transitions for a spin-5/2 nucleus using non-selective rf pulses (the calculated intensities from $M_x^{5,6} = M_x^{1,2}$ and $M_x^{4,5} = M_x^{2,3}$) under different initial conditions.

	Thermal equi.			Invert both ST1s			Invert both sides		
Flip angle	$M_x^{1,2}$	$M_x^{2,3}$	$M_x^{3,4}$	$M_x^{1,2}$	$M_x^{2,3}$	$M_x^{3,4}$	$M_x^{1,2}$	$M_x^{2,3}$	$M_x^{3,4}$
9°	0.39	0.63	0.70	0.75	−0.53	1.98	0.36	−1.10	3.28
18°	0.77	1.24	1.39	1.34	−0.54	3.19	0.57	−1.41	5.22
27°	1.13	1.82	2.04	1.66	0.21	3.30	0.58	−0.56	5.19
36°	1.47	2.35	2.64	1.74	1.51	2.60	0.47	1.11	3.59
45°	1.77	2.83	3.18	1.71	2.87	1.79	0.44	2.82	1.60
54°	2.02	3.23	3.64	1.70	3.77	1.61	0.65	3.78	0.44
63°	2.23	3.56	4.01	1.78	3.94	2.35	1.13	3.61	0.75
72°	2.38	3.80	4.28	1.95	3.54	3.75	1.76	2.60	2.21
81°	2.47	3.95	4.44	2.12	3.00	5.08	2.29	1.48	3.81
90°	2.50	4.00	4.50	2.19	2.75	5.62	2.50	1.00	4.50
Sel-90°	1.12	1.40	1.50			4.50			7.50
	Invert one ST1			Invert $M_z^{1,2}$ then $M_z^{2,3}$					
90°	2.34	3.38	5.06	2.50	2.50	4.50			

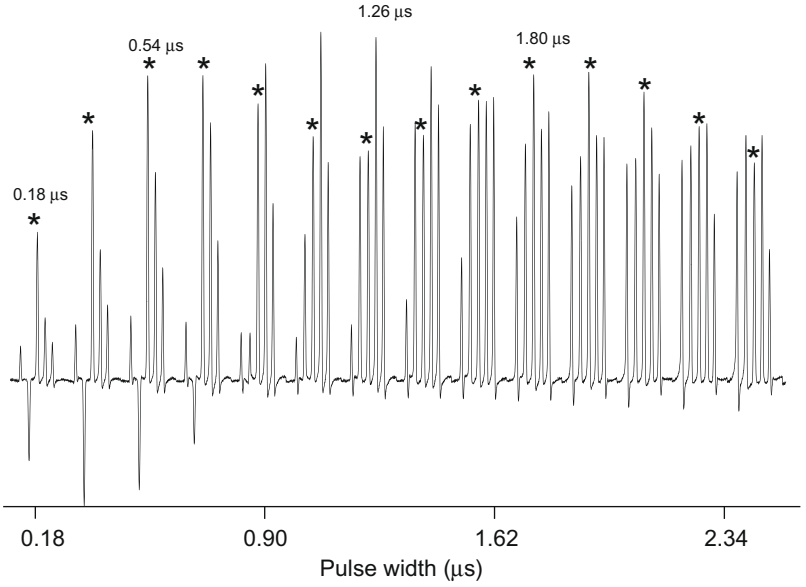

Fig. 5. A series of ^{27}Al NMR spectra of a single crystal of Al_2O_3 with $M_z^{5,6}$ and $M_z^{4,5}$ inverted as a function of pulse width starting at 0.18 μs in 0.18 μs steps (a 90° pulse = 1.8 μs). A single scan is taken per spectrum with a 160 s delay between experiments. The CT in each spectrum is marked with an asterisk.

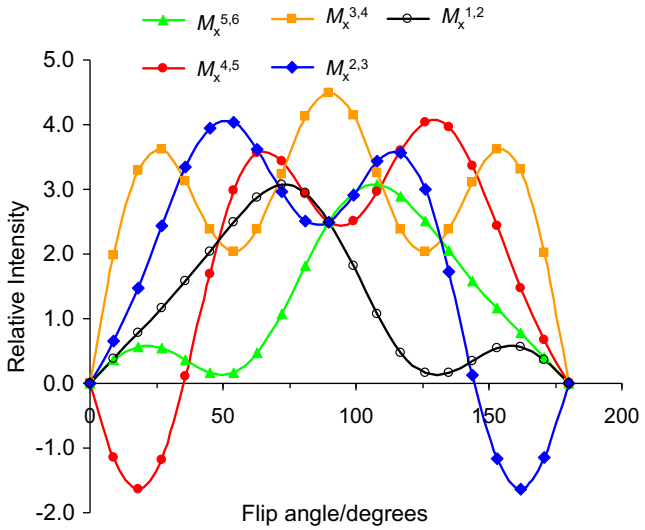

Fig. 6. A plot of the calculated values using density matrices of the intensities of each transition versus the pulse flip angle of a non-selective pulse for a spin-5/2 nucleus beginning with the inversion of $M_z^{5,6}$ and $M_z^{4,5}$.

liquid-state NMR studies [59] while following the dependence of signal intensity on pulse angle in polarization-transfer studies. Use of small flip angles was found to limit the perturbations to the transition that was directly affected by the polarization, whereas the polarization effects observed from read pulse angles greater than 90° were of the opposite sense [59]. The intensity variation of the CT, $M_x^{3,4}$, with a flip angle starting with one side inverted has three maxima at approximately 27°, 90°, and 153° with the maximum at 90° slightly higher in intensity and two minima at pulse angles of about 55° and 125°.

Comparison of the calculated intensities, represented by *x*'s for the CT, $M_x^{3,4}$, for a spin-5/2 nucleus versus the experimentally determined values (Fig. 5), the darkened squares, are shown in Fig. 7. The agreement between theory and experiment for all of the other magnetization components, i.e., $M_x^{1,2}$, $M_x^{2,3}$, $M_x^{4,5}$ and $M_x^{5,6}$ (but not shown) is very good at small pulse angles but not as good at larger values of the pulse angle; however, the overall experimental trends are reproduced by the calculated values. In every case, we found the agreement between experimental versus calculated intensities to be better the higher the rf excitation power level used. However, use of higher power levels than used to acquire the spectra shown here resulted in rf arcing of the probe. The experimental intensity maxima appear to shift toward higher pulse angles and the intensity trough seems to be shallower than the theoretical calculations. SIMPSON calculations indicate that this effect could be reproduced when population inversion was incomplete. It is quite likely that incomplete inversion is present in the experiment because of rf inhomogeneity across the one cm length sample. Moreover, it was found that a larger HS bandwidth (16 kHz) was necessary for the ^{27}Al NMR experiments than used for the ^{23}Na NMR case (HS bandwidth = 2 kHz) even though the resonant separation between the ^{27}Al transitions were approximately 29 kHz while those in ^{23}Na were about 50 kHz. It is not surprising then that HS population inversion might not be as "ideal" in the ^{27}Al NMR case as for the ^{23}Na situation and thus the poorer agreement between theory and experiment for the Al sample.

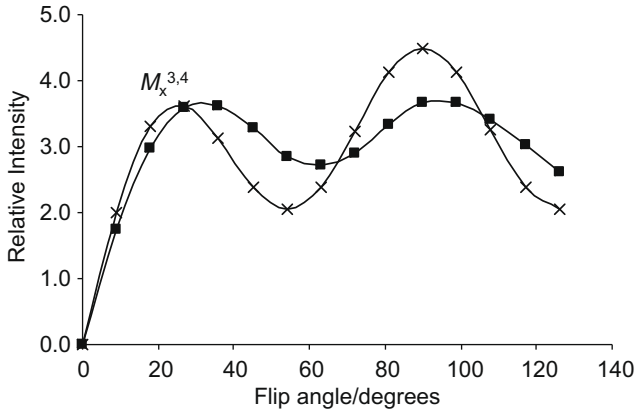

Fig. 7. The calculated intensity for $M_x^{3,4}$ shown as *x*'s versus pulse flip angle for a non-selective pulse, $\gamma B_1/2\pi$ = 138.9 kHz, starting with the inversion of $M_z^{5,6}$ followed immediately with inversion of $M_z^{4,5}$. Experimental points, darkened squares, determined on the ^{27}Al NMR spectrum from a stationary single crystal of sapphire. B_0 = 7.05 T.

4.3. Spin-7/2

For completeness, we show in Table 3 the calculated intensities for each transition using the density matrix approach of a spin-7/2 nucleus as a function of the pulse angle from 0° to 90° using a non-sel. pulse starting with both ST1s inverted and with both sides of the single crystal spectrum inverted. Starting from thermal equilibrium, the ratio of the intensities of each transition observed using a non-sel. 90° pulse is 7.0:12.0:15.0:16.0:15.0:12.0:7.0 as predicted by Schmidt [39]. Also, the ratio of the intensities calculated using a sel. 90° pulse to a non-sel. pulse are almost identical to those reported by Schmidt [39]. As shown in the Table, to obtain maximum CT intensity, 9.82, using non-sel. pulses starting with inversion of both sides of the NMR spectrum of a single crystal, a pulse angle of 18° should be used. When observing the CT with a sel. pulse, for maximum intensity, i.e., 14.0, a 90° sel. pulse should be used with both sides of the NMR spectrum inverted. Shown in Fig. 8 are the plots of the calculated intensities for each transition for a spin-7/2 nucleus as a function of pulse angle from 0° to 180° starting with inversion of the populations of one side of the CT transition (i.e., inversion of $M_z^{1,2}$, followed by inversion of $M_z^{2,3}$ and finally with inversion of $M_z^{3,4}$).

In Fig. 8 the main features are that the magnetizations respond in pairs as was found for the spin-5/2 case. That is, the variations of the intensity with pulse flip angle when $M_z^{1,2}$, $M_z^{2,3}$, and $M_z^{3,4}$ are sequentially inverted prior to the observe pulse, $M_x^{1,2}$ mimics that of $M_x^{7,8}$ except their behavior is a mirror image: similarly for the behavior of the magnetizations of $M_x^{2,3}$ and $M_x^{6,7}$, $M_x^{3,4}$ and $M_x^{5,6}$. Maximum negative intensity for ST1, $M_x^{3,4}$, occurs near 18°, and for its partner, $M_x^{5,6}$, at an angle of 162°. Three maxima occur for the intensity of $M_x^{3,4}$ at angles 50°, 90° and 150° with minima at 18°, 63° and 117°. There are four flip angles which produce the maximum intensity for the CT, namely at 18°, 72°, 108° and 162° with corresponding minima occurring at pulse angles of 40°, 90° and 140°.

Shown in Fig. 9 are the plots of the calculated intensities as a function of pulse flip angle (0–180°) using the density matrix method from a non-sel. pulse for each transition expected for a spin-7/2 nucleus obtained from a single crystal when starting with both sides of the spectrum inverted. The maximum intensity of $M_x^{1,2}$ (also equivalent to $M_x^{7,8}$) occurs at a pulse angle of 90° with inflection points near 36 and 144°; $M_x^{2,3}$ (= $M_x^{6,7}$) has two maxima at angles 63° and 117° with minor maxima at 18° and 162°; $M_x^{3,4}$ (= $M_x^{5,6}$) has three maxima at angles 45°, 90° and 135° with minima at 9° and 171° and also at 63° and 117°; the CT, $M_x^{4,5}$, intensity has four maxima at 18°, 67°, 112° and 162° with corresponding minima at 45°, 90° and 135°.

Table 3
Calculated intensities of the transitions for a spin-7/2 nucleus using selective and non-selective pulses ($M_x^{7,8} = M_x^{1,2}$, $M_x^{6,7} = M_x^{2,3}$, $M_x^{5,6} = M_x^{3,4}$) under different initial conditions.

	Thermal equilibrium							
	$M_x^{1,2}$		$M_x^{2,3}$		$M_x^{3,4}$		$M_x^{4,5}$	
90°	3.5		6.0		7.5		8.0	
Sel-90°	1.3		1.7		1.9		2.0	
	Invert both ST1s				Invert both sides			
Flip angle	$M_x^{1,2}$	$M_x^{2,3}$	$M_x^{3,4}$	$M_x^{4,5}$	$M_x^{1,2}$	$M_x^{2,3}$	$M_x^{3,4}$	$M_x^{4,5}$
9°	0.57	1.73	−0.83	3.31	0.55	0.78	−2.80	7.66
18°	1.20	2.74	−0.01	4.48	1.05	0.84	−2.17	9.82
27°	1.88	2.98	2.46	3.52	1.39	0.51	1.83	6.15
36°	2.44	3.08	4.95	2.56	1.45	0.90	5.75	1.42
45°	2.78	3.64	5.97	3.49	1.32	2.58	6.47	0.48
54°	2.91	4.63	5.60	6.06	1.26	4.75	4.30	3.65
63°	2.93	5.47	5.30	8.24	1.60	5.79	2.44	7.05
72°	2.96	5.69	6.14	8.46	2.35	4.95	3.33	7.28
81°	3.03	5.43	7.66	7.25	3.15	3.16	6.03	4.92
90°	3.06	5.25	8.44	6.50	3.50	2.25	7.50	3.50
Sel-90°				6.00				14.0

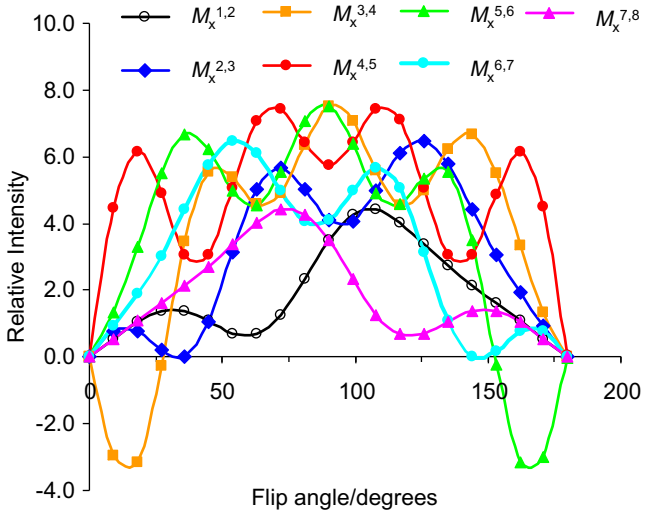

Fig. 8. A plot of the calculated values of the intensities of each transition for a spin-7/2 nucleus as a function of the flip angle from a non-selective pulse beginning with inversion of the populations of the transitions on one side of the central transition (i.e., inversion of $M_z^{1,2}$ followed immediately by inversion of $M_z^{2,3}$, and then $M_z^{3,4}$).

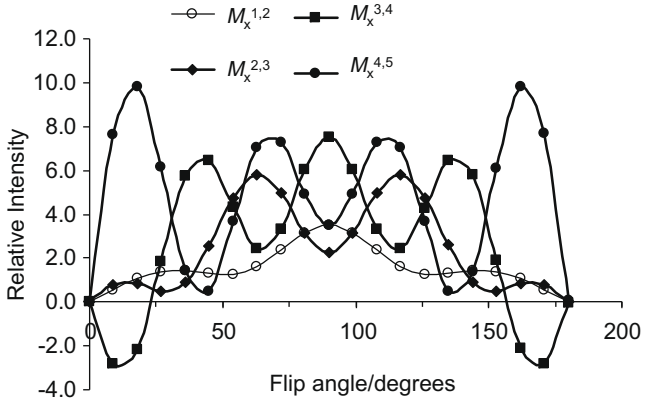

Fig. 9. A plot of the calculated values of the intensities of each transition for a spin-7/2 nucleus as a function of the flip angle from a non-selective pulse beginning with inversion of the populations on both sides (i.e., inversion of $M_z^{1,2}$ and $M_z^{7,8}$ followed immediately by inversion of $M_z^{2,3}$ and $M_z^{6,7}$, and then $M_z^{3,4}$ and $M_z^{5,6}$).

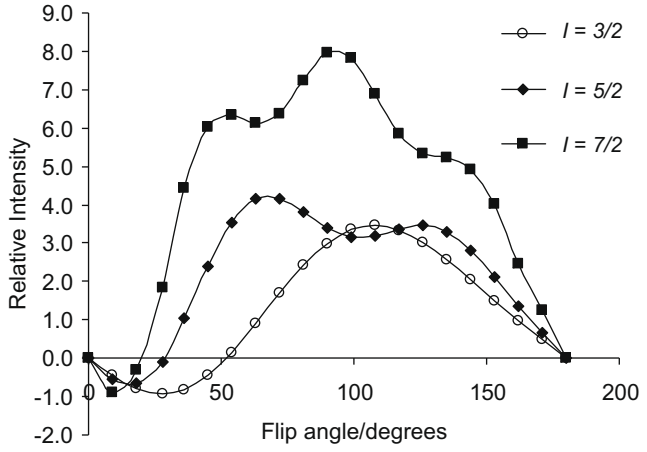

Fig. 10. A plot of the calculated values of the intensities of ST1 ($M_x^{1,2}$, $M_x^{2,3}$ and $M_x^{3,4}$) for spin-3/2, -5/2 and -7/2 nuclei, respectively, shown as open circles, darkened diamonds and darkened squares, respectively, as a function of flip angle starting with inversion of the ST1 ($M_z^{1,2}$, $M_z^{2,3}$ and $M_z^{3,4}$, for spin-3/2, -5/2 and -7/2, respectively).

Finally, shown in Fig. 10 is a plot of the calculated intensities of ST1 as a function of flip angle ranging from 0° to 180° obtained from spin-3/2 ($M_x^{1,2}$), spin-5/2 ($M_x^{2,3}$) and spin-7/2 ($M_x^{3,4}$) nuclei when the populations of this ST1 transition are inverted. The pulse angle resulting in maximum negative intensity from each nucleus for the ST1 transition occur at an angle of 27°, 18° and 9° for spin-3/2, -5/2 and -7/2, respectively. This means that when illustrating the effects of population inversion of nuclear energy states using the NMR spectra from single crystals as test cases, one must be careful of the non-sel. pulse angle used. The results illustrated here indicate that it may be impossible to demonstrate inversion of populations for spin systems with $I > 7/2$ using single crystals.

5. Conclusions

We have shown both experimentally and theoretically that there is an extreme flip-angle dependence of the intensities for each of the transitions of spin-3/2 and -5/2 nuclei when observing the NMR spectra obtained from single crystals applying non-selective pulses to non-equilibrium states. An intensity ratio of approximately 1:0:1 is observed from the ^{23}Na NMR transitions obtained from a single crystal of $NaNO_3$ using a non-selective 90° pulse immediately after inversion of the populations of both satellite transitions. The flip-angle dependence may be reproduced via density matrix calculations. Similarly, for the spin-5/2 nucleus, the flip-angle dependence of the observed intensities from the ^{27}Al NMR spectra of a single crystal of Al_2O_3 may be reproduced with these calculations. It is also shown that to obtain maximum CT intensities the populations of the STs of the NMR spectrum of a single crystal must be inverted sequentially prior to observation with a selective 90° pulse. These conditions may be reproduced quite easily experimentally for single crystals but probably not for powdered samples because of the resulting powder pattern spectrum generated by the orientation dependence of the transition frequencies of the many crystallites within the sample. We include for completeness the theoretical results of the flip-angle dependence obtained from a spin-7/2 nucleus and the Wigner rotation matrix for $I = 9/2$.

We believe that the flip-angle dependence shown here both experimentally and theoretically for single crystals leads to valuable insights into using inversion pulses for sensitivity enhancement of the CT for half-integer spin quadrupolar nuclei in solid-state NMR studies [29]. In particular, this study illustrates that one should use selective 90° pulses in order to obtain the maximum enhancement for the CT using population transfer experiments. As well, we believe the calculations serve as a valuable pedagogical application of density matrix theory.

Acknowledgments

The authors wish to thank members of the solid-state NMR group, particularly Guy Bernard, at the University of Alberta for helpful comments and discussions about this research. We also thank Prof. Alex Bain for helpful discussions, Renée Siegel who was involved in the early stages of this work and Eric Wasylishen for assistance in preparing the figures. We also wish to thank two referees who suggested corrections to the manuscript that improved the readability substantially. R.E.W. is a Canada Research Chair in Physical Chemistry at the University of Alberta and thanks the University of Alberta, the Natural Sciences and Engineering Research Council of Canada (NSERC) and the Government of Canada for research support.

Appendix A. Wigner rotation matrix

A.1. Spin-5/2

C^5	$\sqrt{5}C^4S$	$\sqrt{10}C^3S^2$	$\sqrt{10}C^2S^3$	$\sqrt{5}CS^4$	S^5
$-\sqrt{5}C^4S$	C^5	$2\sqrt{2}C^4S$	$3\sqrt{2}C^3S^2$	$4C^2S^3$	$\sqrt{5}CS^4$
	$-4C^3S^2$	$-3\sqrt{2}C^2S^3$	$-2\sqrt{2}CS^4$	$-S^5$	
$\sqrt{10}C^3S^2$	$3\sqrt{2}C^2S^3$	C^5	$3C^4S$	$3\sqrt{2}C^3S^2$	$\sqrt{10}C^2S^3$
	$-2\sqrt{2}C^4S$	$-6C^3S^2$	$-6C^2S^3$	$-2\sqrt{2}CS^4$	
		$+3CS^4$	$+S^5$		
$-\sqrt{10}C^2S^3$	$3\sqrt{2}C^3S^2$	$-3C^4S$	C^5	$2\sqrt{2}C^4S$	$\sqrt{10}C^3S^2$
	$-2\sqrt{2}CS^4$	$+6C^2S^3$	$-6C^3S^2$	$-3\sqrt{2}C^2S^3$	
		$-S^5$	$+3CS^4$		
$\sqrt{5}CS^4$	S^5	$3\sqrt{2}C^3S^2$	$-2\sqrt{2}C^4S$	C^5	$\sqrt{5}C^4S$
	$-4C^2S^3$	$-2\sqrt{2}CS^4$	$+3\sqrt{2}C^2S^3$	$-4C^3S^2$	
$-S^5$	$\sqrt{5}CS^4$	$-\sqrt{10}C^2S^3$	$\sqrt{10}C^3S^2$	$-\sqrt{5}C^4S$	C^5

A.2. Spin-7/2

C^7	$\sqrt{7}C^6S$	$\sqrt{21}C^5S^2$	$\sqrt{35}C^4S^3$	$\sqrt{35}C^3S^4$	$\sqrt{21}C^2S^5$	$\sqrt{7}CS^6$	S^7
$-\sqrt{7}C^6S$	C^7	$2\sqrt{3}C^6S$	$3\sqrt{5}C^5S^2$	$4\sqrt{5}C^4S^3$	$5\sqrt{3}C^3S^4$	$6C^2S^5$	$\sqrt{7}CS^6$
	$-6C^5S^2$	$-5\sqrt{3}C^4S^3$	$-4\sqrt{5}C^3S^4$	$-3\sqrt{5}C^2S^5$	$-2\sqrt{3}CS^6$	$-S^7$	
$\sqrt{21}C^5S^2$	$-2\sqrt{3}C^6S$	$-10C^5S^2$	$\sqrt{15}C^6S$	$2\sqrt{15}C^5S^2$	$10C^4S^3$	$5\sqrt{3}C^3S^4$	$\sqrt{21}C^2S^5$
	$+5\sqrt{3}C^4S^3$	$+10C^3S^4$	$-4\sqrt{15}C^4S^3$	$-4\sqrt{15}C^3S^4$	$-10C^2S^5$	$-2\sqrt{3}CS^6$	
		$+C^7$	$+2\sqrt{15}C^2S^5$	$+\sqrt{15}CS^6$	$+S^7$		
$-\sqrt{35}C^4S^3$	$3\sqrt{5}C^5S^2$	$-\sqrt{15}C^6S$	C^7	$4C^6S$	$2\sqrt{15}C^5S^2$	$4\sqrt{5}C^4S^3$	$\sqrt{35}C^3S^4$
	$-4\sqrt{5}C^3S^4$	$+4\sqrt{15}C^4S^3$	$-12C^5S^2$	$-18C^4S^3$	$-4\sqrt{15}C^3S^4$	$-3\sqrt{5}C^2S^5$	
		$-2\sqrt{15}C^2S^5$	$+18C^3S^4$	$+12C^2S^5$	$+\sqrt{15}CS^6$		
			$-4CS^6$	$-S^7$			
$\sqrt{35}C^3S^4$	$-4\sqrt{5}C^4S^3$	$2\sqrt{15}C^5S^2$	$-4C^6S$	C^7	$\sqrt{15}C^6S$	$3\sqrt{5}C^5S^2$	$\sqrt{35}C^4S^3$
	$+3\sqrt{5}C^2S^5$	$-4\sqrt{15}C^3S^4$	$+18C^4S^3$	$-12C^5S^2$	$-4\sqrt{15}C^4S^3$	$-4\sqrt{5}C^3S^4$	
		$+\sqrt{15}CS^6$	$-12C^2S^5$	$+18C^3S^4$	$+2\sqrt{15}C^2S^5$		
			$+S^7$	$-4CS^6$			
$-\sqrt{21}C^2S^5$	$5\sqrt{3}C^3S^4$	$-10C^4S^3$	$2\sqrt{15}C^5S^2$	$-\sqrt{15}C^6S$	$-10C^5S^2$	$2\sqrt{3}C^6S$	$\sqrt{21}C^5S^2$
	$-2\sqrt{3}CS^6$	$+10C^2S^5$	$-4\sqrt{15}C^3S^4$	$+4\sqrt{15}C^4S^3$	$+10C^3S^4$	$-5\sqrt{3}C^4S^3$	
		$-S^7$	$+\sqrt{15}CS^6$	$-2\sqrt{15}C^2S^5$	$+C^7$		
$\sqrt{7}CS^6$	$-6C^2S^5$	$5\sqrt{3}C^3S^4$	$-4\sqrt{5}C^4S^3$	$3\sqrt{5}C^5S^2$	$-2\sqrt{3}C^6S$	C^7	$\sqrt{7}C^6S$
	$+S^7$	$-2\sqrt{3}CS^6$	$+3\sqrt{5}C^2S^5$	$-4\sqrt{5}C^3S^4$	$+5\sqrt{3}C^4S^3$	$-6C^5S^2$	
$-S^7$	$\sqrt{7}CS^6$	$-\sqrt{21}C^2S^5$	$\sqrt{35}C^3S^4$	$-\sqrt{35}C^4S^3$	$\sqrt{21}C^5S^2$	$-\sqrt{7}C^6S$	C^7

A.3. Spin 9/2

C^9	$3C^8S$	$6C^7S^2$	$2\sqrt{21}C^6S^3$	$3\sqrt{14}C^5S^4$	$3\sqrt{14}C^4S^5$	$2\sqrt{21}C^3S^6$	$6C^2S^7$	$3CS^8$	S^9
	C^9	$4C^8S$	$2\sqrt{21}C^7S^2$	$4\sqrt{14}C^6S^3$	$5\sqrt{14}C^5S^4$	$4\sqrt{21}C^4S^5$	$14C^3S^6$	$8C^2S^7$	
$-3C^8S$	$-8C^7S^2$	$-14C^6S^3$	$-4\sqrt{21}C^5S^4$	$-5\sqrt{14}C^4S^5$	$-4\sqrt{14}C^3S^6$	$-2\sqrt{21}C^2S^7$	$-4CS^8$	$-S^9$	$3CS^8$
		C^9	$\sqrt{21}C^8S$	$3\sqrt{14}C^7S^2$	$5\sqrt{14}C^6S^3$	$5\sqrt{21}C^5S^4$	$21C^4S^5$		
	$-4C^8S$	$-14C^7S^2$	$-6\sqrt{21}C^6S^3$	$-10\sqrt{14}C^5S^4$	$-10\sqrt{14}C^4S^5$	$-6\sqrt{21}C^3S^6$	$-14C^2S^7$	$14C^3S^6$	
$6C^7S^2$	$+14C^6S^3$	$+21C^5S^4$	$+5\sqrt{21}C^4S^5$	$+5\sqrt{14}C^3S^6$	$+3\sqrt{14}C^2S^7$	$+\sqrt{21}CS^8$	$+S^9$	$-4CS^8$	$6C^2S^7$
			C^9	$2\sqrt{6}C^8S$	$5\sqrt{6}C^7S^2$	$20C^6S^3$			
		$-\sqrt{21}C^8S$	$-18C^7S^2$	$-15\sqrt{6}C^6S^3$	$-20\sqrt{6}C^5S^4$	$-45C^4S^5$	$5\sqrt{21}C^5S^4$		
	$2\sqrt{21}C^7S^2$	$+6\sqrt{21}C^6S^3$	$+45C^5S^4$	$+20\sqrt{6}C^4S^5$	$+15\sqrt{6}C^3S^6$	$+18C^2S^7$	$-6\sqrt{21}C^3S^6$	$4\sqrt{21}C^4S^5$	
$-2\sqrt{21}C^6S^3$	$-4\sqrt{21}C^5S^4$	$-5\sqrt{21}C^4S^5$	$-20C^3S^6$	$-5\sqrt{6}C^2S^7$	$-2\sqrt{6}CS^8$	$-S^9$	$+\sqrt{21}CS^8$	$-2\sqrt{21}C^2S^7$	$2\sqrt{21}C^3S^6$
				C^9	$5C^8S$				
			$-2\sqrt{6}C^8S$	$-20C^7S^2$	$-40C^6S^3$	$5\sqrt{6}C^7S^2$			
		$3\sqrt{14}C^7S^2$	$+15\sqrt{6}C^6S^3$	$+60C^5S^4$	$+60C^4S^5$	$-20\sqrt{6}C^5S^4$	$5\sqrt{14}C^6S^3$		
	$-4\sqrt{14}C^6S^3$	$-10\sqrt{14}C^5S^4$	$-20\sqrt{6}C^4S^5$	$-40C^3S^6$	$-20C^2S^7$	$+15\sqrt{6}C^3S^6$	$-10\sqrt{14}C^4S^5$	$5\sqrt{14}C^5S^4$	
$3\sqrt{14}C^5S^4$	$+5\sqrt{14}C^4S^5$	$+5\sqrt{14}C^3S^6$	$+5\sqrt{6}C^2S^7$	$+5CS^8$	$+S^9$	$-2\sqrt{6}CS^8$	$+3\sqrt{14}C^2S^7$	$-4\sqrt{14}C^3S^6$	$3\sqrt{14}C^4S^5$
				$-5C^8S$	C^9				
			$5\sqrt{6}C^7S^2$	$+40C^6S^3$	$-20C^7S^2$	$2\sqrt{6}C^8S$			
		$-5\sqrt{14}C^6S^3$	$-20\sqrt{6}C^5S^4$	$-60C^4S^5$	$+60C^5S^4$	$-15\sqrt{6}C^6S^3$	$3\sqrt{14}C^7S^2$		
	$5\sqrt{14}C^5S^4$	$+10\sqrt{14}C^4S^5$	$+15\sqrt{6}C^3S^6$	$+20C^2S^7$	$-40C^3S^6$	$+20\sqrt{6}C^4S^5$	$-10\sqrt{14}C^5S^4$	$4\sqrt{14}C^6S^3$	
$-3\sqrt{14}C^4S^5$	$-4\sqrt{14}C^3S^6$	$-3\sqrt{14}C^2S^7$	$-2\sqrt{6}CS^8$	$-S^9$	$+5CS^8$	$-5\sqrt{6}C^2S^7$	$+5\sqrt{14}C^3S^6$	$-5\sqrt{14}C^4S^5$	$3\sqrt{14}C^5S^4$
			$-20C^6S^3$	$5\sqrt{6}C^7S^2$	$-2\sqrt{6}C^8S$	C^9			
		$5\sqrt{21}C^5S^4$	$+45C^4S^5$	$-20\sqrt{6}C^5S^4$	$+15\sqrt{6}C^6S^3$	$-18C^7S^2$	$\sqrt{21}C^8S$		
	$-4\sqrt{21}C^4S^5$	$-6\sqrt{21}C^3S^6$	$-18C^2S^7$	$+15\sqrt{6}C^3S^6$	$-20\sqrt{6}C^4S^5$	$+45C^5S^4$	$-6\sqrt{21}C^6S^3$	$2\sqrt{21}C^7S^2$	
$2\sqrt{21}C^3S^6$	$+2\sqrt{21}C^2S^7$	$+\sqrt{21}CS^8$	$+S^9$	$-2\sqrt{6}CS^8$	$+5\sqrt{6}C^2S^7$	$-20C^3S^6$	$+5\sqrt{21}C^4S^5$	$-4\sqrt{21}C^5S^4$	$2\sqrt{21}C^6S^3$
		$-21C^4S^5$	$5\sqrt{21}C^5S^4$	$-5\sqrt{14}C^6S^3$	$3\sqrt{14}C^7S^2$	$-\sqrt{21}C^8S$	C^9		
	$14C^3S^6$	$+14C^2S^7$	$-6\sqrt{21}C^3S^6$	$+10\sqrt{14}C^4S^5$	$-10\sqrt{14}C^5S^4$	$+6\sqrt{21}C^6S^3$	$-14C^7S^2$	$4C^8S$	
$-6C^2S^7$	$-4CS^8$	$-S^9$	$+\sqrt{21}CS^8$	$-3\sqrt{14}C^2S^7$	$+5\sqrt{14}C^3S^6$	$-5\sqrt{21}C^4S^5$	$+21C^5S^4$	$-14C^6S^3$	$6C^7S^2$
	$-8C^2S^7$	$14C^3S^6$	$-4\sqrt{21}C^4S^5$	$5\sqrt{14}C^5S^4$	$-4\sqrt{14}C^6S^3$	$2\sqrt{21}C^7S^2$	$-4C^8S$	C^9	
$3CS^8$	$+S^9$	$-4CS^8$	$+2\sqrt{21}C^2S^7$	$-4\sqrt{14}C^3S^6$	$+5\sqrt{14}C^4S^5$	$-4\sqrt{21}C^5S^4$	$+14C^6S^3$	$-8C^7S^2$	$3C^8S$
$-S^9$	$3CS^8$	$-6C^2S^7$	$2\sqrt{21}C^3S^6$	$-3\sqrt{14}C^4S^5$	$3\sqrt{14}C^5S^4$	$-2\sqrt{21}C^6S^3$	$6C^7S^2$	$-3C^8S$	C^9

References

[1] A.D. Bain, Radiofrequency pulses: response of nuclear spins, in: D.M. Grant, R.K. Harris (Eds.), Encyclopedia of Nuclear Magnetic Resonance, vol. 6, John Wiley & Sons, Chichester, England, 1996, pp. 3944–3949.

[2] R.R. Ernst, W.A. Anderson, Application of Fourier transform spectroscopy to magnetic resonance, Rev. Sci. Instrum. 37 (1966) 93–102.

[3] R.R. Ernst, G. Bodenhausen, A. Wokaun, Principles of Nuclear Magnetic Resonance in One and Two Dimensions, Clarendon Press, Oxford, 1987.

[4] T.C. Farrar, E.D. Becker, Pulse and Fourier Transform NMR Introduction to Theory and Methods, Academic Press, New York and London, 1971.

[5] R. Freeman, D.H. Whiffen, Determination of the relative signs of proton spin coupling constants by double irradiation, Mol. Phys. 4 (1961) 321–325.

[6] R.E.D. McClung, N.R. Krishna, Fourier transform double resonance NMR on two- and three-spin systems, J. Magn. Reson. 29 (1978) 573–585.

[7] R.A. Hoffman, S. Forsén, High resolution nuclear magnetic double and multiple resonance, in: J.W. Emsley, J. Feeney, L.H. Sutcliffe (Eds.), Progress in Nuclear Magnetic Resonance Spectroscopy, vol. 1, Pergamon Press, Toronto, 1966, pp. 15–205.

[8] R. Freeman, S. Wittekoek, R.R. Ernst, High-resolution NMR study of relaxation mechanisms in a two-spin system, J. Chem. Phys. 52 (1970) 1529–1544.

[9] N.R. Krishna, S.L. Gordon, Intermolecular nuclear Overhauser studies of coupled spin systems in high resolution NMR, J. Chem. Phys. 58 (1973) 5687–5696.

[10] G.L. Closs, L.E. Closs, Induced dynamic nuclear spin polarization in reactions of photochemically and thermally generated triplet diphenylmethylene, J. Amer. Chem. Soc. 91 (1969) 4549–4550.

[11] J. Bargon, H. Fischer, Nuclear magnetic resonance emission lines during fast radical reactions. II. Chemically induced dynamic nuclear polarization, Z. Naturforschung 22 (1967) 1556–1562.

[12] R. Siegel, T.T. Nakashima, R.E. Wasylishen, Signal enhancement of NMR spectra of half-integer quadrupolar nuclei in solids using hyperbolic secant pulses, Chem. Phys. Lett. 388 (2004) 441–445.

[13] R. Siegel, T.T. Nakashima, R.E. Wasylishen, Sensitivity enhancement of NMR spectra of half-integer spin quadrupolar nuclei in solids using hyperbolic secant pulses, J. Magn. Reson. 184 (2007) 85–100.

[14] R.W. Schurko, I. Hung, C.M. Widdifield, Signal enhancement in NMR spectra of half-integer quadrupolar nuclei via DFS-QCPMG and RAPT-QCPMG pulse sequences, Chem. Phys. Lett. 379 (2003) 1–10.

[15] Z. Yao, H.-T. Kwak, D. Sakellariou, L. Emsley, P.J. Grandinetti, Sensitivity enhancement of the central transition NMR signal of quadrupolar nuclei under magic-angle spinning, Chem. Phys. Lett. 327 (2000) 85–90.

[16] A.P.M. Kentgens, R. Verhagen, Advantages of double frequency sweeps in static, MAS and MQMAS NMR of spin $I = 3/2$ nuclei, Chem. Phys. Lett. 300 (1999) 435–443.

[17] D. Iuga, H. Schäfer, R. Verhagen, A.P.M. Kentgens, Population and coherence transfer induced by double frequency sweeps in half-integer quadrupolar spin systems, J. Magn. Reson. 147 (2000) 192–209.

[18] D. Iuga, A.P.M. Kentgens, Influencing the satellite transitions of half-integer quadrupolar nuclei for the enhancement of magic angle spinning spectra, J. Magn. Reson. 158 (2002) 65–72.

[19] J. Haase, M.S. Conradi, Sensitivity enhancement for NMR of the central transition of quadrupolar nuclei, Chem. Phys. Lett. 209 (1993) 287–291.

[20] J. Haase, M.S. Conradi, E. Oldfield, Single- and double-resonance experiments of quadrupolar nuclei in solids using sensitivity enhancement of the central transition, J. Magn. Reson. A 109 (1994) 210–215.

[21] S. Schäublin, A. Höhener, R.R. Ernst, Fourier spectroscopy of nonequilibrium states: application to CIDNP, Overhauser experiments and relaxation time measurements, J. Magn. Reson. 13 (1974) 196–216.

[22] P. Meakin, J.P. Jesson, Computer simulation of multipulse and Fourier transform NMR experiments. IV. Some simulations including the time development of the off-diagonal density matrix elements, J. Magn. Reson. 18 (1975) 411–426.
[23] A.D. Bain, J.S. Martin, FT NMR of nonequilibrium states of complex spin systems. I. A Liouville space description, J. Magn. Reson. 29 (1978) 125–135.
[24] P.L. Wessels, R. Pachter, Homonuclear selective population inversion. The AB system, J. Magn. Reson. 38 (1980) 365–367.
[25] D. Canet, J. Brondeau, J.-P. Marchal, H. Nery, Selective pulses applied to multiplets in homonuclear-coupled NMR spectra; Determination of mutual coupling, J. Magn. Reson. 36 (1979) 35–51.
[26] G. Bodenhausen, R. Freeman, Pulse cascades: a simple description of the flip angle dependence of NMR spectra, J. Magn. Reson. 36 (1979) 221–226.
[27] A.P.M. Kentgens, Off-resonance nutation nuclear magnetic resonance spectroscopy of half-integer quadrupolar nuclei, Prog. NMR Spect. 32 (1998) 141–164.
[28] A. Samoson, E. Lippmaa, Central transition NMR excitation spectra of half-integer quadrupole nuclei, Chem. Phys. Lett. 100 (1983) 205–208.
[29] N.M. Trease, K.K. Dey, P.J. Grandinetti, Optimum excitation of "enhanced" central transition populations, J. Magn. Reson. 200 (2009) 334–339.
[30] N.M. Trease, P.J. Grandinetti, Solid-state nuclear magnetic resonance in the rotating tilted frame, J. Chem. Phys. 128 (2008) 052318-1-12.
[31] M. Garwood, L. DelaBarre, The return of the frequency sweep: designing adiabatic pulses for contemporary NMR, J. Magn. Reson. 153 (2001) 155–177.
[32] E. Kupče, R. Freeman, Stretched adiabatic pulses for broadband spin inversion, J. Magn. Reson. A 117 (1995) 246–256.
[33] E. Kupče, R. Freeman, Optimized adiabatic pulses for wideband spin inversion, J. Magn. Reson. A 118 (1996) 299–303.
[34] M.S. Silver, R.I. Joseph, C.-N. Chen, V.J. Sank, D.I. Hoult, Selective population inversion in NMR, Nature 310 (1984) 681–683.
[35] M.S. Silver, R.I. Joseph, D.I. Hoult, Highly selective Pi/2 and Pi pulse generation, J. Magn. Reson. 59 (1984) 347–351.
[36] M.S. Silver, R.I. Joseph, D.I. Hoult, Selective spin inversion in nuclear magnetic resonance and coherent optics through an exact solution of the Bloch-Riccati equation, Phys. Rev. A 31 (1985) 2753–2755.
[37] A. Tannús, M. Garwood, Adiabatic pulses, NMR Biomed. 10 (1997) 423–434.
[38] Y.A. Tesiram, M.R. Bendall, Universal equations for linear adiabatic pulses and characterization of partial adiabaticity, J. Magn. Reson. 156 (2002) 26–40.
[39] V.H. Schmidt, Pulse response in the presence of quadrupolar splitting, Proc. Ampere Int. Summer School II (1971) 75–83.
[40] P.P. Man, J. Klinowski, A. Trokiner, H. Zanni, P. Papon, Selective and non-selective NMR excitation of quadrupolar nuclei in the solid state, Chem. Phys. Lett. 151 (1988) 143–150.
[41] M.H. Levitt, Spin Dynamics Basics of Nuclear Magnetic Resonance, second ed., John Wiley and Sons Ltd., Chichester, England, 2008.
[42] A. Abragam, Principles of Nuclear Magnetism, Clarendon Press, Oxford, 1986.
[43] E. Fukushima, S.B.W. Roeder, Experimental Pulse NMR: A Nuts and Bolts Approach, Addison-Wesley, Publishing Co. Inc., Reading, Massachusetts, 1981.
[44] T.C. Farrar, Density matrices in NMR spectroscopy: Part I, Concepts Magn. Reson. 1990 (1990) 1–12.
[45] T.C. Farrar, Density matrices in NMR spectroscopy: Part II, Concepts Magn. Reson. 1990 (1990) 55–61.
[46] S. Vega, Fictitious spin 1/2 operator formalism for multiple quantum NMR, J. Chem. Phys. 68 (1978) 5518–5527.
[47] S. Vega, A. Pines, Operator formalism for double quantum NMR, J. Chem. Phys. 66 (1977) 5624–5644.
[48] A. Wokaun, R.R. Ernst, Selective excitation and detection in multilevel spin systems: application of single transition operators, J. Chem. Phys. 67 (1977) 1752–1758.
[49] E. Van Veenendaal, B.H. Meier, A.P.M. Kentgens, Frequency stepped adiabatic passage excitation of half-integer quadrupolar spin systems, Mol. Phys. 93 (1998) 195–213.
[50] P.P. Man, Quadrupolar couplings in nuclear magnetic resonance: general, in: R.A. Meyers (Ed.), Encyclopedia of Analytical Chemistry, vol. 14, John Wiley & Sons, Tarzana California, 2000, pp. 12224–12265.
[51] P.J. Hore, J.A. Jones, S. Wimperis, NMR: The Toolkit, vol. 92, Oxford University Press, Oxford, 2000.
[52] P.P. Man, Numerical analysis of Hahn echoes in solids, Phys. Rev. B 52 (1995) 9418–9426.
[53] D. Freude, J. Haase, Quadrupolar effects in solid-state nuclear magnetic resonance, in: P. Diehl, E. Fluck, H. Gunter, R. Kosfeld, J. Seelig (Eds.), NMR Basic Principles and Progress, vol. 29, Springer-Verlag, Berlin, 1993, pp. 1–90.
[54] M.E. Rose, Elementary Theory of Angular Momentum, John Wiley & Sons, New York, 1957.
[55] M.H. Levitt, mPackages version 4.6.
[56] K.K. Dey, S. Prasad, J.T. Ash, M. Deschamps, P.J. Grandinetti, Spectral editing in solid-state MAS NMR of quadrupolar nuclei using selective satellite inversion, J. Magn. Reson. 185 (2007) 326–330.
[57] M. Bak, J.T. Rasmussen, N.C. Nielsen, SIMPSON: A general simulation program for solid-state NMR spectroscopy, J. Magn. Reson. 147 (2000) 296–330.
[58] P.A. Keifer, 90 degree pulse width calibrations: How to read a pulse width array, Concepts Magn. Reson. 11 (1999) 165–180.
[59] W.S. Brey, Basic methods and simple pulsed experiments, in: W.S. Brey (Ed.), Pulsed Methods in 1D and 2D Liquid-Phase NMR, Academic Press, Inc., San Diego, California, 1987, pp. 1–109.